Open access • Posted Content • DOI:10.1101/2020.04.24.057588

Investigation of a night soil compost psychrotrophic bacterium Glutamicibacter arilaitensis LJH19 for its safety, efficient hydrolytic and plant growth-promoting potential — Source link

Shruti Sinai Borker, Shruti Sinai Borker, Aman Thakur, Aman Thakur ...+4 more authors

Institutions: Council of Scientific and Industrial Research, Academy of Scientific and Innovative Research

Published on: 25 Apr 2020 - bioRxiv (Cold Spring Harbor Laboratory)

Topics: Psychrotrophic bacteria

Investigation of a night soil compost psychrotrophic bacterium *Glutamicibacter arilaitensis* LJH19 for its safety, efficient hydrolytic and plant growth-promoting potential

Shruti Sinai Borker[1,2], Aman Thakur[1,2], Sanjeet Kumar[1], Sareeka Kumari[1], Rakshak Kumar[1]*, Sanjay Kumar[1]

[1]Biotechnology Division, CSIR-Institute of Himalayan Bioresource Technology Palampur, Himachal Pradesh, 176061, India.

[2]Academy of Scientific and Innovative Research (AcSIR), CSIR-Inst. of Himalayan Bioresource Technology, Palampur, Himachal Pradesh, India

***Corresponding author**:

Dr Rakshak Kumar,
Scientist, Biotechnology Division,
CSIR-Institute of Himalayan Bioresource Technology,
Palampur, Himachal Pradesh, 176061, India.
Email: rakshak@ihbt.res.in, rakshakacharya@gmail.com
Tel.: +91 1894 233339 (ext. 441)
Fax: +91 1894 230433

Abstract

Night soil compost (NSC) has traditionally been a source of organic manure in north-western Himalaya. Lately, this traditional method is declining due to modernization, its unhygienic conditions and social apprehensions. Reduction in the age-old traditional practice has led to excessive usage of chemical fertilizers and shortage of water in the eco-sensitive region. Microbiological intervention was attempted to obtain bacterial consortia for accelerated degradation of human faeces in cold climate to improvise this traditional knowledge. *Glutamicibacter arilaitensis* LJH19, a psychrotrophic bacteria was identified as one such potential candidate for the proposed consortia. The bacterium was isolated from NSC of Lahaul valley and exhibited potential hydrolytic activities, the specific activities of amylase, cellulase and xylanase was observed as 186.76 U/mg, 21.85 U/mg and 11.31 U/mg respectively. Additionally, the strain possessed multiple plant growth-promoting (PGP) traits. The bacterium produced 166.11 µg/ml indole acetic acid and 85.72 % siderophore units, and solubilized 44.76 µg/ml phosphate. Whole genome sequence (3,602,821 bps) endorsed the cold adaptation, polysaccharide metabolism, PGP potential of the bacterium. Genome mining revealed biosynthetic gene clusters for type III polyketide synthase (PKS), terpene, and siderophore in agreement with its potential PGP traits. Comparative genomics within the genus revealed 217 unique genes specific to hydrolytic and PGP activity. Negative haemolysis and biofilm production and susceptibility towards all 12 tested antibiotics indicated the bacterium to be a safe bioinoculant. Genomic investigation supported the bacterium safety with absence of any virulence and antibiotic resistance genes. We propose the strain LJH19 to be a potentially safe bioinoculant candidate for efficient degradation of night soil owing to its survivability in cold and its efficient hydrolytic and PGP potential.

Keywords: Winter dry toilet, amylase, indole acetic acid, siderophore, type III PKS

Introduction

The highland agro system of north-western Himalaya lacks productivity and soil fertility due to extreme weather conditions like heavy snowfall, avalanches, landslides, soil erosion, and scanty rainfall (Kuniyal et al., 2004). To increase soil fertility and meet the high demand for manure, traditional winter dry toilets (Fig. 1A) are prevalent in this region. It is a unique traditional method of composting night soil (human excreta) and involves the use of agricultural and household waste locally called '*fot*,' to cover faeces after defecation (Fig. 1B) (Oinam *et al.,* 2008). The resultant manure is supplemented in the fields to sustain the agro-ecosystem (Indian science wire, 2019; Oinam *et al.,* 2008). However, due to the effect of modernization and the introduction of modern septic toilets, the practice of dry toilets and night soil composting is nearing demise. Other factors such as foul odour, availability of subsidized chemical fertilizers, rise in the standard of living, the difficulty of finding labour and social apprehensions have also contributed to the decline of the age-old practice (Oinam et al., 2008). For decades this age-old practice of night soil compost (NSC) have conserved water during severe winter and the organic manure formed have sustained the agro-ecosystem. Now due to abandoning this practice, there is excessive use of chemical fertilizers and shortage of water in the region for agriculture purpose. Maintaining the agro-ecosystem, conserving water and promoting dry toilets in the region is of utmost priority. It was suggested to combine the scientific knowledge with traditional dry toilets so that the practice becomes safer and hygienic (Oinam et al*.,* 2008). However, we failed to retrieve any literature support on any scientific intervention addressing this problem.

Microbial involvement for rapid decomposition in a cold climate (below 20°C) using psychrotrophic bacterial consortium has been emphasized earlier (Hou et al., 2017). Here, a psychrotrophic bacterial community weighs special attention to accelerate the biodegradation process in night soil composting. The lower microbial load in the initial composting process delays the mesophilic phase due to slower biomass degradation resulting in a shorter thermophilic phase (Hou et al., 2017). These conditions subsequently affect the maturity of compost and risks safety and contamination (Millner et al., 2014).

Plant growth-promoting bacteria (PGPB) also plays an important role in maintaining soil fertility. It directly stimulates plant growth by increasing the availability of the nutrients, often found in the form which is unutilized by the plants such as iron, nitrogen, and phosphorous (de Souza et al., 2015). PGPB also produces phytohormones (indole acetic

acid), growth regulators (siderophores) and solubilise phosphate to modulate plant growth and development (Numan et al., 2018). The use of PGPB thus gains importance, for sustenance and supporting the agro-ecosystem of Lahaul valley.

Pathogenicity was the main concern while exploring night-soil compost (NSC) for potential psychrotrophic bacteria. Human faeces are known to contain large amounts of enteric microorganisms and many opportunistic pathogens (Heinonen-Tanski and van Wijk-Sijbesma, 2005). The low ambient temperature of the Lahaul region and lower metabolic activity of microbial load might increase the possibilities of poor thermal inactivation of pathogenic strains in NSC. Such a scenario promotes the chances of low-level contamination of pathogenic strains. Apparently, this expresses the worry about the potential of isolated bacterial strains to have harmful impacts on the human, environment, and crop health (Avery et al., 2012).

In the course of finding potential non-pathogenic, hydrolytic and plant growth-promoting (PGP) psychrotrophic bacteria from NSC, we obtained a bacterial strain LJH19 that showed remarkable PGP traits and considerable capabilities of hydrolytic activity in *in-vitro* assays. Owing to its cold adaptation, efficient hydrolytic activity, PGP potential, and origin from faecal compost, whole-genome sequencing was performed to elucidate the genetic basis of the catabolic activities, PGP traits, and analysis for pathogenicity determinants. Further, to explore the habitat-specific gene repertoire, we performed comparative genomics of LJH19 with all the available strains of same genus. On the basis of a unique genome region across the strain LJH19, a comparison was withdrawn with the closely related strains. Biosynthetic gene clusters in the genome of LJH19 were also identified and further to evaluate bacterial safety, the presence of antibiotic resistance gene cluster across all the strains was assessed. To the best of our knowledge, this is first such a report from NSC of north-western Himalaya on bacterial safety and its functional characteristics.

Materials and method

Sampling source, strain isolation and hydrolytic potential

NSC samples were collected from the collection chamber of night-soil composting toilet, locally termed as “Ghop” of Jundah village (32.64°N 76.84°E) of Lahaul valley (Fig. 1C). The samples were collected from the core of the compost pile in sterile plastic bottles using stainless steel spatula in triplicates and stored in ice box containing ice packs. The samples were then immediately transported to the laboratory, and processed. The temperature was

noted at the time of sampling itself by inserting the handheld digital thermometer (model: ST9269, MEXTECH, India) into the core of the compost pile. Air dried solid sample was mixed with milli-Q at a ratio of 1:10 vortexed and were kept overnight to check pH and electrical conductivity (EC) using digital pH and EC meter (Eutech, India). For the analysis of total available nitrogen, phosphorus and potassium, the samples were dried at room temperature, finely grounded and sieved. All the chemical analysis was performed as per the standard methods for testing of compost materials (TMECC, 2002).

The bacterial strain LJH19 was isolated from NSC samples while screening for potential psychrotrophic hydrolytic bacteria. The isolation was carried out using serial dilution method and spread plate method on nutrient agar (NA) medium (HiMedia) at 15°C. The bacterial isolation was performed in the Class II, Type A2 Biological Safety Cabinet (Thermo Scientific™). The optimum growth conditions of the LJH19 strain were determined by incubating the culture at various temperatures (4-50°C), NaCl concentration (1-10%), and pH (2 to 10) range. The production of hydrolytic enzymes by the LJH19 strain was initially screened using a plate assay method. The exponentially grown culture of LJH19 was spot inoculated on Carboxymethylcellulose (CMC) agar (Kasana et al., 2008), Starch agar (Hi-Media), Xylan agar (Alves-Prado et al., 2010), Tributyrin agar (Hi-Media) plates and incubated at 15°C for 48 hrs. The clear halo zones around the colony indicated positive results. The enzymatic index (EI=Diameter of the halo of hydrolysis/Diameter of the colony) was calculated as described previously by Vermelho and Couri, 2013. For quantitative estimation of polysaccharide degrading enzymes viz. cellulase, xylanase, and amylase, the microplate-based 3, 5-dinitrosalicylic acid colorimetry method was followed using 1% (w/v) carboxymethylcellulose (CMC), 1% birchwood xylan (HiMedia) and 1% soluble starch (HiMedia) as the substrate (Xiao et al., 2005).

Haemolysin and protease assay, biofilm formation and antibiotic susceptibility profile

For assessment of pathogenic potential, we assayed LJH19 for protease and haemolysin activity using a plate assay method (Igbinosa et al., 2017). The strains *Staphylococcus aureus* subsp. aureus (MTCC 96), *Bacillus subtilis* (MTCC121), *Escherichia coli* (MTCC 43), *Micrococcus luteus* (MTCC 2470) were used as a positive control for haemolytic activity. Haemolytic activity was interpreted according to Buxton, (2016).

Biofilm formation was evaluated according to Basson and Igbinosa (Basson et al., 2008; Igbinosa et al., 2017).) with slight modifications. The cells adhered were stained with 200 µL of 0.5% crystal violet for 10 min. The optical density (OD) readings from respective wells

were obtained at 595 nm. The cutoff OD (ODc) for the test was set using the formula (Mean OD of negative control + 3x Standard deviation) and results were interpreted as previously described by Basson et al., (2008). The wells containing only TSB broth (200 µL) served as negative control while the well-containing strains Staphylococcus aureus subsp. aureus (MTCC 96), Bacillus subtilis (MTCC121), Escherichia coli (MTCC 43), Micrococcus luteus (MTCC 2470) was used as a positive control. The test organisms were characterized as non-biofilm producers (OD<ODC), weak (ODC < OD< 2ODc), intermediate (2ODc < OD< 4ODc), and strong (OD>4ODc).

Antibiotic susceptibility profiling was carried out by using the Kirby-Bauer method (Bauer et al., 1966). The antibiotic discs (HiMedia) used were 15 mcg, Azithromycin (AZM); 10 mcg, Ampicillin (AMP); 5 mcg, Ciprofloxacin (CIP); 30 mcg, Chloramphenicol (CHL); 15 mcg Erythromycin (E); 10 mcg, Gentamycin (G); 30 mcg, Kanamycin (K); 10 Units, Penicillin-G (P); 5 mcg, Rifampicin (RIF); 10 mcg, Streptomycin (S); 30 mcg, Tetracycline (TE); 30 mcg, Vancomycin (VA). The plates were incubated at 15°C for 48 hrs. Zones of clearance was measured in millimetre (mm) and interpreted as Resistant, Intermediate or Sensitive using guidelines provided by the manufacturer.

Plant growth-promoting (PGP) attributes

Indole acetic acid (IAA) production by LJH19 was studied according to Goswami et al., (2014) by supplementing the nutrient broth (100 ml) with L-Trytophan (200 µg ml−1). Siderophore production by LJH19 was initially screened on Chrome Azurol Sulphonate (CAS) agar at 15°C (Lynne et al., 2011). Quantitative estimation of siderophore was done using CAS-shuttle assay (Goswami et al., 2014) by growing LJH19 in iron-free CAS-broth (pH 6.8) at 15°C at 150 rpm. Ammonia production was quantified spectrophotometrically (Cappuccino. and Sherman, 2014). LJH19 was grown in peptone water at 15°C for 10 days at 150 rpm. Inorganic phosphate solubilisation was estimated by the vanado-molybdate method (Gulati et al., 2010) using NBRIP broth containing 0.5% tricalcium phosphate (TCP).

Strain identification, phylo-taxono-genomics, and gene content analysis

The genomic DNA was extracted using the conventional CTAB method (William et al., 2004) and for identification, partial 16S rRNA gene sequencing of V1 and V9 regions using 27F and 1492R primers, was performed. To provide a genetic basis to the experimental evidence, we performed whole-genome sequencing using PacBio RS-II (Pacific Biosciences, US) as previously described (Himanshu et al., 2016; Kumar et al., 2015). The draft genome sequence was deposited in NCBI GenBank with accession number SPDS00000000. Strain

identification was done at the species level using EzTaxon (https://www.ezbiocloud.net/identify). Manual curation of the genomes from a public repository for the closest match was performed with NCBI Genome (https://www.ncbi.nlm.nih.gov/genome/?term=Glutamicibacter). Genome quality was assessed using CheckM v1.1.2 (Parks et al., 2015) in terms of its completeness and contamination present.

Strain phylogeny was assessed using the 16S rRNA gene sequence as well as whole-genome phylogeny using PhyloPhlAn v0.99 (Segata et al., 2013). For the construction of the 16S rRNA gene phylogenetic tree, all the full-length 16S rRNA reported strains of genus *Glutamicibacter* were used. *Micrococcus luteus* (Nucleotide accession No: AF542073) was used as an outgroup. The 16S rRNA gene phylogenetic tree was constructed using ClustalX v2.1 (Larkin et al., 2007) and FastTree v2.1.8 (Price et al., 2010) with default parameters. Whole-genome phylogeny was constructed using PhyloPhlAN (It uses a 400 most conserved gene across bacterial domains and constructs its phylogeny). All the genomes (Table 2) were annotated using prokka v1.14.6 (Seemann, 2014). The orthoANI v1.2 (Yoon et al., 2017) was performed to infer the taxonomic relatedness of the strain LJH19. ANI value matrix obtained was used for generating heatmap using the webserver of Morpheus (https://software.broadinstitute.org/morpheus). Further, 10 strains forming a clade were considered for pan-genome analysis with a 95% cutoff using Roary v3.6.0 (Page et al., 2015). The unique gene present in the strain LJH19 was fetched and annotated with eggNOG mapper v1 (Powell et al., 2014) (http://eggnogdb.embl.de/app/home#/app/home). Chromosomal maps (Alikhan et al., 2011) for comparison of the closely related strains and visualization of the unique genomic region across the strain LJH19 to the type strain RE117 and JB182 are marked in the figure (Fig. 3).

To identify the biosynthetic gene clusters (BGCs) in genome *G. arilaitensis* LJH19, we used a web-based server of antiSMASH v5.0 (https://antismash.secondarymetabolites.org/#!/start) (Blin et al., 2019) and cluster image of the identified biosynthetic gene was prepared with EASYfig v2.2.2 (Sullivan et al., 2011). To assess the presence of the antibiotic gene cluster across the strains, a web-based server of Resistance gene identifier (RGI) v5.1.0 module of Comprehensive Antibiotic Resistance Database (CARD) v3.0.8 (Alcock et al., 2020) was used with strict mode. The pathogenic potential of LJH19 was also assessed using the PathogenFinder web service under automated mode (Cosentino et al., 2013).

Results and Discussion

Physico-chemical properties of NSC samples and bacterial characterisation

Sampling in triplicate was conducted from the collection chamber of the traditional night soil toilet "*ghop*". The temperature of the sample was noted to be 9.9°C at the core of the pile. The pH value of the compost sample was observed to be 10, while the electrical conductivity (EC) noted was 1674 µS. The available nitrogen, phosphorous and potassium in the NSC sample was 2297.6 ± 99.4 ppm, 117.11 ± 0.34 ppm, and 22534.11 ± 73.08 ppm respectively.

In an attempt to explore the bacterial diversity of NSC, we isolated 130 bacterial strains belonging to different phyla (unpublished data). In this study, the hydrolytic potential of an opaque, yellow-pigmented bacterium LJH19 was determined on agar plates (Table 1) which showed significant activity for different substrates viz. corn starch, CMC and birchwood xylan (Fig. S1) (Table 1). To further characterize this bacterium, partial 16S rRNA gene sequencing was performed, which gave best hit with *G. arilaitensis* Re117 with 100% identity and coverage of 96.5% in EzTaxon Biocloud (https://www.ezbiocloud.net/identify). The 16S rRNA partial gene sequence was deposited in the NCBI through BankIt web-based sequence submission tool under accession number MT349443.

Hydrolytic activity and plant growth promoting attributes of LJH19

The biodegradation of complex polysaccharide by bacteria requires a cocktail of enzymes to depolymerize it to oligosaccharides and monomer sugars (Awasthi et al., 2015). Amylases plays a crucial role in hydrolysis of starchy molecules which specifically acts on alpha-1,4-glycosidic linkages to yield maltose, D-glucose, dextrins and shorter oligosaccharides (Jurado et al., 2015). Quantitatively, LJH19 showed the production of amylase enzyme with specific activity of 186.76 ± 19.28 U/mg (Fig. S2) using corn starch as substrate. Similarly, LJH19 also exhibited the production of cellulase enzyme with specific activity of 21.85 ± 0.7 U/mg (Fig. S2) using CMC as a substrate at 15°C. Cellulase enzyme is involved in hydrolysis of cellulose and hemicellulose, which are the major constituent of plant cell wall (Kostylev and Wilson, 2012). Previous studies (Aarti et al., 2018; Aarti et al., 2017) also found that *G. arilaitensis* strain ALA4 exhibit efficient amylase and cellulase activity. This evidence supports the capability of LJH19 to produce the amylase and cellulase enzyme.

Biodegradation of hemicelluloses is attained by the collective action of a variety of hydrolytic enzymes (Chandra et al., 2015). Since xylan is the major polysaccharide found in hemicelluloses, xylan β-(1, 4)-xylosidase plays a key role in its degradation. In addition to cellulase, LJH19 also showed the production of xylanase enzyme with specific activity of

11.31± 0.51 U/mg (Fig. S2) using birchwood xylan as a substrate at 15°C. Based on these results LJH19 presents the considerable potential of hydrolysing complex polysaccharides (starch, cellulose and xylan) which are the major constituents of residues used in NSC while surviving under low ambient temperature. It is critical for a bacterium to thrive in cold regions as well as to perform collectively, ensuring efficient composting (Hou et al., 2017).

During the process of decomposition, a large number of nutrients are released (Biswas and Kole, 2017). These nutrients are lost from agricultural systems due to leaching, surface runoff and eutrophication, eventually remaining unavailable for plant uptake (Adesemoye and Kloepper, 2009). The plant growth-promoting bacteria (PGPB) aids in improving nutrient uptake and increases the efficiency of applied compost. It plays a pivotal role as biofertilizers since they promote plant growth in a nutrient-limited soil by improving the nutrient availability, and phytohormone production (Dey et al., 2004). Since, soil temperature at high altitude regions remains low, indigenous cold-tolerant bacterium possessing plant growth-promoting (PGP) activities would play an important role in the enhancement of soil nutrients and their utilization by the host plant. Keeping this in consideration, bacterium LJH19 was further evaluated for different PGP attributes (Table 1) (Fig. S3).

Siderophore production by PGPB is also vital for plant defense. Iron chelation by siderophores suppresses fungal pathogens in the rhizosphere (Gulati et al., 2009). In our study, LJH19 was grown in the iron-free CAS broth with pH 6.8 and exhibited considerable siderophore production of 85.72 ±1.06 percent siderophore unit (psu) at 15°C. Further to determine the chemical nature of siderophore, we examined the absorption maxima (λmax) of cell-free supernatant in UV-3092 UV/Visible spectrophotometer. We observed a peak at 292nm in the absorption spectra (Fig. S4). In previous study, it was reported that in acidic medium 2,3-dihydroxybenzoic acid (DHB), a phenolic compound consisting of catechol group which absorbs below 330 nm showing two absorption bands with maxima at 254 nm and 292 nm, respectively (Iglesias et al., 2011). DHB is an intermediate involved in the synthesis of catecholate type siderophore (Peralta et al., 2016). These evidences support the presence of DHB in LJH19 grown supernatant indicating the production of catecholate type siderophore.

Production of phytohormone IAA is essential for plant growth to proliferate lateral roots and root hairs (Rosier et al., 2018). In this study, LJH19 demonstrated the ability to produce 166.11 ± 5.7 µg/ml of IAA by colorimetric assay after 72 Hrs of incubation with 200 µg/ml

concentration of L-Trytophan at 15°C (Fig. S3A). This infers the ability of LJH19 to produce the IAA in the presence of L-tryptophan signifying the tryptophan dependent pathway of auxin production.

Phosphorous (P) plays an essential role in plant growth and its solubilisation by the action of microorganisms is regarded as the vital PGP trait (Oteino et al., 2015). Since, the plant is unable to uptake inorganic phosphate present in fixed or precipitated form in the soil, bacteria aids in increasing the availability of soluble P for plant acquisition through solubilisation (Santos-Beneit, 2015). Qualitative estimation of phosphate solubilisation showed a 2.3 solubilisation index. Quantitatively, LJH19 was able to solubilise 44.76 ± 1.5 µg/ml of tri-calcium phosphate at 15°C after the 5th day of incubation in NBRIP broth (Fig. S3C). The activity of bacteria was able to decrease pH from 7 to 4.5 indicating the elevation of phosphate solubilisation levels. This suggested that the presence of LJH19 in the compost can deliver available phosphorous to the plants.

Ammonia production by bacteria is yet another feature of PGPB to increase the availability of nitrogen by mineralising organic nitrogen into ammonia (Karthika et al., 2020). In our in-vitro assays, the isolate LJH19 was able to produce a low level of ammonia production (0.20± 0.01 µmoles/ml) (Fig. S3B) after 10 days of incubation in peptone water. These values are quite low in the case of PGP attributes. But, in the case of composting, ammonia gas released by bacteria is primarily responsible for pungent smell and loss of organic nitrogen from the compost (Zhou et al., 2019). This may suggest that it doesn't directly benefit the plants but may be able to maintain stable organic nitrogen content in the compost by not converting rich nitrogenous sources into ammonia gas.

Phylogenetic assessment and genome relatedness

A phylogenetic construction based on the complete 16S rRNA gene sequences of a strain belonging to genus *Glutamicibacter* suggests the closest relative of strain LJH19. It was found closest to strain *G. arilaitensis* JB182 but, the type strain of the genus falls in a separate clade (Fig. 2A). The true phylogeny of the isolate was obtained with the phylogenomic tree obtained from PhyloPhlAn, which uses around 400 most conserved gene sequences present across the isolates. Strain LJH19, type strain Re117 and JB182 was found to be in a single clade (Fig. 2B). In order to get the genome relatedness estimate, we have implemented the orthoANI estimation of the isolates from the genus. ANI matrix suggests the

genome similarity of the strain LJH19 to subspecies level relatedness to the strain Re117 as its value was around 97% for the type strain Re117 and another strain JB182 (Fig. 2C).

Pan-genome analysis and Chromosomal map

Roary run for the group of the strains forming a clade with the type strain of *Glutamicibacter arilaitensis* and LJH19 resulted in a pan-genome of 9892 genes. A total of 634 genes were found to be core genes, whereas the gene clusters specific to the strain LJH19, Re117 and BJ182 was 1740. A total of 217 genes were specific to the strain LJH19. Chromosomal map showing the unique genomic regions across the strain LJH19 depicts the uniqueness of the strain LJH19 (Fig. 3A). All the strain-specific gene from LJH19 classified by eggNOG falls in several COG categories (Fig. 3B). List of the unique gene, its function and COG classification is reported in Table S2. Based on data retrieved from Prokka annotation and unique genes retrieved from roary run, a representative figure illustrating an overview of different genes involved in catabolic activities, transport, and plant growth promotion in *G. arilaitensis* LJH19 was generated (Fig. 4).

Extended genomic insights on hydrolytic and plant growth promoting attributes of LJH19

The *actinobacteria* are very well known for their ability to produce a variety of secondary metabolites (Dinesh et al., 2017). Hence, we searched for secondary metabolites gene clusters using antiSMASH v5.0 (Blin et al., 2019). This resulted in the identification of three biosynthetic gene cluster namely type III polyketide synthase (PKS), terpene, and siderophore (Fig. 6). The most significant hit predicted by the antiSMASH for type III PKS, terpenes and siderophore is dechlorocuracomycin, carotenoid and desferrioxamin B/desferrioxamine E respectively. Type III PKS are involved in the synthesis of numerous metabolites and have a variety of biological and physiological roles such as defense systems in bacteria (Shimizu et al., 2017). The presence carotenoid gene cluster supports the indicative yellow color of the LJH19 colonies. Besides pigmentation, the major function of carotenoids in bacteria is to protect the cell from UV radiations, oxidative damage and modify membrane fluidity (Liao et al., 2019).

The occurrence of the siderophore gene cluster is demonstrated by the experimental evidence of the *in-vitro* CAS-shuttle assay (Goswami et al., 2014). Through genome mining, we also identified some genes involved in the synthesis of polyamines (PAs), Putrescine (Put) and

spermidine (Spd) (TableS2). In bacteria, these active molecules are involved in the biosynthesis of siderophores, improve the survival rate in freezing conditions, and stabilize spheroplasts and protoplasts from osmotic shock (Wortham et al., 2007).

As we discussed earlier, experimental evidence results suggested that LJH19 is involved in the catecholate type siderophore production. The genomic insights further strengthened these findings by predicting the genes involved in the biosynthesis of enterobactin and petrobactin. However, antiSMASH predicted gene clusters for hydroxamate type desferrioxamine B/E siderophore. These results deduce that LJH19 may be able to produce a wide variety of siderophores. Most of the enzymes involved in enterobactin biosynthesis were present except the genes involved in the conversion of 2,3-Dihydro-2,3-dihydroxybenzoate to enterobactin (Fig. 4) (Table S1). We also noticed the genes encoding the transporters required for the import and export of synthesized enterobactin. In respect to the biosynthesis of petrobactin, spermidine molecules are used for synthesis using citrate backbone (Budzikiewicz, 2005). However, no genes were identified in LJH19 for the synthesis of petrobactin. Nevertheless, we identified the genes encoding the transporters required for the import and export of both synthesized enterobactin and petrobactin (Fig. 5) (Table S1). In addition to this, we also found transporters for hydroxamate type siderophores (Table S1). These results correlate with the desferrioxamin B/desferrioxamine E gene cluster identified in antiSMASH run.

A series of genes related to other PGP traits were also identified in the LJH19 genome, the candidate genes that are likely involved in tryptophan-dependent IAA biosynthesis via indole-3-acetamide (IAM) pathway, such as amidase that converts IAM to IAA was present in the genome. However, gene encoding L-tryptophan monooxygenase was missing which converts L-tryptophan to IAM (Li et al., 2018). We also found few genes encoding phosphatases, inositol-phosphatases, and gluconate permease in the genome of LJH19 (Table S1) involved in P metabolism. LJH19 strain has also been noted to carry genes involved in nitrate/nitrite transport pathways including the genes associated with denitrification and nitrate reduction like nitrite reductase and nitrate reductase. Nitrite reductase encoded by the NirD gene converts nitrite to ammonium and further converted to glutamate by glutamate synthetase for amino acid metabolism. These results suggest that LJH19 can deliver plants with available nitrogen sources via enzymatic conversion.

LJH19 strain has several genes encoding proteins involved in the metabolism of a wide variety of complex polysaccharides (Table S1). The depolymerisation of polysaccharides into

its oligosaccharides and monomer sugars by bacteria requires a combination of enzymes (Tutino et al., 2002). Many genes in the LJH19 encoded beta-glucosidase, alpha-amylase, beta-xylosidase, pullulanase, oligo-1,6-glucosidase and glycosidases which are involved in the degradation of polysaccharides like cellulose, starch, and xylan (Fig. 4).

The endo-acting enzymes such as alpha-amylase initially hydrolyse the internal linkages of the starch molecule randomly liberating linear and branched oligosaccharides. The pullulanase enzyme specifically cleaves alpha-(1,6)-linkage in pullulan and branched oligosaccharides releasing maltodextrin. Cellulases cleaves the β-(1,4)-glycosidic linkages within the cellulose polymer releasing cellobiose and glucose. Xylan β-(1, 4)-xylosidase cleaves xylan polymers generating smaller oligosaccharides and xylose monomers (Chandra, 2016). Finally, monomeric sugars like glucose and xylose delivered to the cell cytoplasm through specific transporters enter into the glycolysis pathway and ultimately to the TCA cycle generating energy for cellular growth. LJH19 strain have all the crucial genes involved in the core metabolic pathways like glycolysis, citric acid cycle (TCA), gluconeogenesis and pentose phosphate pathway (Fig. 4). LJH19 is also well-equipped with genes encoding proteins that are components of transporter complexes engaged in the recognition and transport of monosaccharide and oligosaccharide such as maltose/maltodextrin, maltooligosaccharide, and cellobiose and transporters for hydrolysed proteins as well (Table S1). Furthermore, we also observed genes such as triacylglycerol lipase which is associated with fatty acid degradation.

LJH19 also harboured several genes related to the adaptational approaches (Table S3). Several cold associated genes encoding for proteins responsible for cold-active chaperons, general stress, osmotic stress, oxidative stress, membrane/cell wall alteration, carbon storage/ starvation, DNA repair, Toxin/Antitoxin modules were identified across the genome. These results infer survival strategies in cold environments.

In vitro and *in silico* pathogenicity analysis of LJH19

LJH19 strain had shown remarkable PGP potential and appreciable hydrolytic activity at low temperature but, to ensure bacterial safety for humans, we determined the pathogenic properties of LJH19 isolate (Table 1). The present study focused on determining the virulence in humans associated with components involved in their colonization into host cells, essential for the commencement of infection. Pathogenic bacteria rely on a variety of virulence factors

394 to induce pathogenesis including adhesion proteins, toxins like haemolysins and proteases
395 (Martínez-García et al., 2018). We performed the initial screening of virulence on blood agar
396 to check the haemolytic activity. In this plate assay, we noticed no haemolytic activity for
397 LJH19 in contrast to haemolytic strains MTCC 96, MTCC121, MTCC 43, MTCC 2470 (Fig.
398 S5A). LJH19 was tested positive for protease activity with an enzymatic index of 12.5 (Fig.
399 S5B), but, quantitatively LJH19 showed very low protease activity (Table 1).

400 Furthermore, the adherence of bacteria to the host tissue cells is the initial step to induce the
401 pathogenesis (Wilson *et al.,* 2019). Therefore, biofilm formation is a notable virulence factor
402 of pathogenic potential. In our in-vitro assay, LJH19 was not able to form biofilm on
403 polystyrene at 37°Cbut, was a weak biofilm producer at 15°C (Fig. S5C). In addition to
404 pathogenesis, biofilm formation also infers antibiotic resistance to the bacterial cells
405 (Patterson et al., 2010). Therefore, we also checked for the resistance phenotype of LJH19,
406 which showed susceptibility to all the twelve antibiotics tested (Fig. S5D), (Table 1).

407 Virulence is a characteristic of pathogenicity which confers the ability to initiate and sustain
408 infection for the organism. The occurrence of such determinants at the genetic level makes
409 the organism potentially pathogenic with the ability to circulate such genes in the bacterial
410 population (Igbinosa et al., 2017). Since, LJH19 showed some resistance to four antibiotics
411 (Table 1) in our *in-vitro* assays, to affirm the antibiotic resistance obtained from *in-vitro*
412 *assays* we performed an *insilico* investigation of LJH19 genome and its phylogenetic relative.
413 But, the RGI module of CARD 2020 with strict mode resulted in the detection of no
414 antibiotic resistance gene cluster in LJH19 and its relatives. To further confirm these results,
415 we also assessed the LJH19 genome for its pathogenic potential by PathogenFinder. This
416 web-based tool identifies the genome and provides a probability measure for the test strain to
417 be pathogenic for humans. The predicted results identified LJH19 as a non-human pathogen
418 with an average probability of 0.228 (Supplementary file S4). No putative virulence or
419 pathogenic genes were identified. These results suggested no traces of pathogenicity in
420 LJH19.

421 **Conclusion**

422 Night soil compost is a rich nutrient source and when supplemented to the soil increases its
423 fertility. In this study, *G. arilaitensis* LJH19 isolated from NSC demonstrated the ability of
424 hydrolysing complex polysaccharides richly found in agricultural residues like starch,

cellulose and xylan. The bacterium also exhibited several PGP traits such as IAA production, siderophore production and phosphate solubilization at low ambient temperature. A comprehensive genomic analysis further predicted and excavated some key genes related to the cold adaptation, polysaccharide metabolism, and plant growth promotion. LJH19 also displayed its capabilities as safe bioinoculant by demonstrating negative haemolysis and biofilm formation. Genomic search reinforced the bacterium's safety with absence of any virulence and antibiotic resistance genes. These results indicated that *G. arilaitensis* LJH19 may serve as a safe bioinoculant and may work collectively in a consortium for efficiently degrading night soil as well as enrich the soil with its PGP attributes. To the best of our knowledge, the current study is the pioneering scientific intervention addressing the issue of NSC in high Himalaya.

Author statement

Shruti Sinai Borker: Methodology, Validation, Data curation, Writing- Original draft **Aman Thakur**: Methodology, Writing- Original draft preparation **Sanjeet Kumar**: Software, Writing- Original draft **Sareeka Kumari**: Methodology **Rakshak Kumar**: Conceptualization, Writing - Review & Editing, Supervision, Funding acquisition **Sanjay Kumar**: Project administration

Acknowledgment

SSB is thankful to UGC, Govt. of India for 'Research Fellowship' Grant [UGC-Ref.No.:461/ (CSIR-UGC NET DEC. 2016)]. This work was financially supported by the CSIR in-house FTT project (MLP 0137) and the NMHS project of MoEF&CC (NMHS sanction no. GBPNI/NMHS-2018-19/SG/178). Authors also duly acknowledge the technical support provided by Anil Chaudhary for 16S rRNA gene sequencing, Mohit Kumar Swarnkar for whole genome sequencing and Dr. Vishal Acharya for genome assembly. Authors also acknowledge Aman Kumar for his technical assistance in figure generation. This manuscript represents CSIR-IHBT communication no. **4602**

References

Aarti, C., Khusro, A., Agastian, P., 2018a. Carboxymethyl cellulase production optimization from *Glutamicibacter arilaitensis* strain ALA4 and its application in lignocellulosic waste biomass saccharification. Preparative Biochemistry and Biotechnology 48, 853–866. https://doi.org/10.1080/10826068.2018.1514513

456 Aarti, C., Khusro, A., Agastian, P., 2017. Goat dung as a feedstock for hyper-production of
457 amylase from *Glutamicibacter arilaitensis* strain ALA4. Bioresources and
458 Bioprocessing 4. https://doi.org/10.1186/s40643-017-0174-4

459 Adesemoye, A.O., Kloepper, J.W., 2009. Plant-microbes interactions in enhanced fertilizer-
460 use efficiency. Applied Microbiology and Biotechnology 85, 1–12.
461 https://doi.org/10.1007/s00253-009-2196-0

462 Alves-Prado, H.F., Pavezzi, F.C., Leite, R.S.R., de Oliveira, V.M., Sette, L.D., DaSilva, R.,
463 2010. Screening and production study of microbial xylanase producers from Brazilian
464 Cerrado. Applied Biochemistry and Biotechnology 161, 333–346.
465 https://doi.org/10.1007/s12010-009-8823-5

466 Alcock, B.P., Raphenya, A.R., Lau, T.T.Y., Tsang, K.K., Bouchard, M., Edalatmand, A.,
467 Huynh, W., Nguyen, A.L. v., Cheng, A.A., Liu, S., Min, S.Y., Miroshnichenko, A.,
468 Tran, H.K., Werfalli, R.E., Nasir, J.A., Oloni, M., Speicher, D.J., Florescu, A., Singh,
469 B., Faltyn, M., Hernandez-Koutoucheva, A., Sharma, A.N., Bordeleau, E., Pawlowski,
470 A.C., Zubyk, H.L., Dooley, D., Griffiths, E., Maguire, F., Winsor, G.L., Beiko, R.G.,
471 Brinkman, F.S.L., Hsiao, W.W.L., Domselaar, G. v., McArthur, A.G., 2020. CARD
472 2020: antibiotic resistome surveillance with the comprehensive antibiotic resistance
473 database. Nucleic acids research 48, D517–D525. https://doi.org/10.1093/nar/gkz935

474 Alikhan, N.F., Petty, N.K., ben Zakour, N.L., Beatson, S.A., 2011. BLAST Ring Image
475 Generator (BRIG): Simple prokaryote genome comparisons. BMC Genomics 12.
476 https://doi.org/10.1186/1471-2164-12-402

477 Arif, M.S., Riaz, M., Shahzad, S.M., Yasmeen, T., Ashraf, M., Siddique, M., Mubarik, M.S.,
478 Bragazza, L., Buttler, A., 2018. Fresh and composted industrial sludge restore soil
479 functions in surface soil of degraded agricultural land. Science of the Total Environment
480 619–620, 517–527. https://doi.org/10.1016/j.scitotenv.2017.11.143

481 Awasthi, M.K., Pandey, A.K., Bundela, P.S., Khan, J., 2015. Co-composting of organic
482 fraction of municipal solid waste mixed with different bulking waste: Characterization of
483 physicochemical parameters and microbial enzymatic dynamic. Bioresource Technology
484 182, 200–207. https://doi.org/10.1016/j.biortech.2015.01.104

485 Basson, A., Flemming, L.A., Chenia, H.Y., 2008. Evaluation of adherence, hydrophobicity,
486 aggregation, and biofilm development of *Flavobacterium* johnsoniae-like isolates.
487 Microbial Ecology 55, 1–14. https://doi.org/10.1007/s00248-007-9245-y

488 Bauer, A., Kirby, W.M.M., Sherris, J.C., 1966. turck, Turck M. Antibiotic susceptibility
489 testing by a standardized single disk method. American journal of clinical pathology 45,
490 493.

491 Bertoldo, C., Antranikian, G., 2002. Starch-hydrolysing enzymes from thermophilic archaea
492 and bacteria. Current opinion in chemical biology 6, 151–160.

493 Biswas, T., Kole, S.C., 2017. Soil Organic Matter and Microbial Role in Plant Productivity
494 and Soil Fertility 219–238. https://doi.org/10.1007/978-981-10-7380-9_10

495 Blin, K., Shaw, S., Steinke, K., Villebro, R., Ziemert, N., Lee, S.Y., Medema, M.H., Weber,
496 T., 2019. antiSMASH 5.0: updates to the secondary metabolite genome mining pipeline.
497 Nucleic acids research 47, W81–W87. https://doi.org/10.1093/nar/gkz310

498 Budzikiewicz, H., 2005. Bacterial Citrate Siderophores. Mini-Reviews in Organic Chemistry
499 2, 119–124. https://doi.org/10.2174/1570193053544436

500 Bunsangiam, S., Sakpuntoon, V., Srisuk, N., Ohashi, T., Fujiyama, K., Limtong, S., 2019.
501 Biosynthetic Pathway of Indole-3-Acetic Acid in *Basidiomycetous* Yeast
502 *Rhodosporidiobolus fluvialis*. Mycobiology 47, 292–300.
503 https://doi.org/10.1080/12298093.2019.1638672

504 Buxton, R., 2016. Blood Agar Plates and Haemolysis Protocols 1–9.

505 Cappuccino., J.G., Sherman, N., 2014. New Features Make the Micro Lab More Clinical
506 Application Gram Staining : The First, Clinical application.

507 Chandra, R., Yadav, S., Kumar, V., 2015. Microbial degradation of lignocellulosic waste and
508 its metabolic products. Environmental waste management 249–298.

509 Chassard, C., Goumy, V., Leclerc, M., Del'homme, C., Bernalier-Donadille, A., 2007.
510 Characterization of the xylan-degrading microbial community from human faeces.
511 FEMS Microbiology Ecology 61, 121–131. https://doi.org/10.1111/j.1574-
512 6941.2007.00314.x

513 Cheong, W.H., Tan, Y.C., Yap, S.J., Ng, K.P., 2015. ClicO FS: An interactive web-based
514 service of Circos. Bioinformatics 31, 3685–3687.
515 https://doi.org/10.1093/bioinformatics/btv433

516

517 de Souza, R., Ambrosini, A., Passaglia, L.M.P., 2015. Plant growth-promoting bacteria as
518 inoculants in agricultural soils. Genetics and Molecular Biology 38, 401–419.
519 https://doi.org/10.1590/S1415-475738420150053

520 Dey, R., Pal, K.K., Bhatt, D.M., Chauhan, S.M., 2004. Growth promotion and yield
521 enhancement of peanut (*Arachis hypogaea* L.) by application of plant growth-promoting
522 *rhizobacteria*. Microbiological Research 159, 371–394.
523 https://doi.org/10.1016/j.micres.2004.08.004

524 Dinesh, R., Srinivasan, V., Sheeja, T.E., Anandaraj, M., Srambikkal, H., 2017. Endophytic
525 actinobacteria: Diversity, secondary metabolism and mechanisms to unsilence
526 biosynthetic gene clusters. Critical Reviews in Microbiology 43, 546–566.
527 https://doi.org/10.1080/1040841X.2016.1270895

528 Duca, D., Lorv, J., Patten, C.L., Rose, D., Glick, B.R., 2014. Indole-3-acetic acid in plant-
529 microbe interactions. Antonie van Leeuwenhoek, International Journal of General and
530 Molecular Microbiology 106, 85–125. https://doi.org/10.1007/s10482-013-0095-y

531 Dutta, S., Wu, K.C.W., 2014. Enzymatic breakdown of biomass: Enzyme active sites,
532 immobilization, and biofuel production. Green Chemistry 16, 4615–4626.
533 https://doi.org/10.1039/c4gc01405g

534 Goswami, D., Dhandhukia, P., Patel, P., Thakker, J.N., 2014. Screening of PGPR from saline
535 desert of Kutch: Growth promotion in Arachis hypogea by *Bacillus licheniformis* A2.
536 Microbiological Research 169, 66–75. https://doi.org/10.1016/j.micres.2013.07.004

537 Gulati, A., Sharma, N., Vyas, P., Sood, S., Rahi, P., Pathania, V., Prasad, R., 2010. Organic
538 acid production and plant growth promotion as a function of phosphate solubilisation by
539 *Acinetobacter rhizosphaerae* strain BIHB 723 isolated from the cold deserts of the trans-
540 Himalayas. Archives of Microbiology 192, 975–983. https://doi.org/10.1007/s00203-
541 010-0615-3

542 Gulati, A., Vyas, P., Rahi, P., Kasana, R.C., 2009. Plant growth-promoting and rhizosphere-
543 competent *Acinetobacter rhizosphaerae* strain BIHB 723 from the cold deserts of the
544 Himalayas. Current Microbiology 58, 371–377. https://doi.org/10.1007/s00284-008-
545 9339-x

546 Hagan, A.K., Carlson, P.E., Hanna, P.C., 2016. Flying under the radar: The non-canonical
547 biochemistry and molecular biology of petrobactin from *Bacillus anthracis*. Molecular
548 Microbiology 102, 196–206. https://doi.org/10.1111/mmi.13465

549 Hagan, A.K., Tripathi, A., Berger, D., Sherman, D.H., Hanna, P.C., 2017. Petrobactin is
550 exported from Bacillus anthracis by the RND-type exporter ApeX. MBio 8, e01238-17.

551 Himanshu, Swarnkar, M.K., Singh, D., Kumar, R., 2016. First complete genome sequence of
552 a species in the genus *Microterricola*, an extremophilic cold active enzyme producing
553 bacterial strain ERGS5:02 isolated from Sikkim Himalaya. Journal of Biotechnology
554 222, 17–18. https://doi.org/10.1016/j.jbiotec.2016.02.011

555 Hou, N., Wen, L., Cao, H., Liu, K., An, X., Li, D., Wang, H., Du, X., Li, C., 2017. Role of
556 psychrotrophic bacteria in organic domestic waste composting in cold regions of China.
557 Bioresource Technology 236, 20–28. https://doi.org/10.1016/j.biortech.2017.03.166

558 Igbinosa, I.H., Beshiru, A., Odjadjare, E.E., Ateba, C.N., Igbinosa, E.O., 2017. Pathogenic
559 potentials of *Aeromonas* species isolated from aquaculture and abattoir environments.
560 Microbial Pathogenesis 107, 185–192. https://doi.org/10.1016/j.micpath.2017.03.037

561 Iglesias, E., Brandariz, I., Jiménez, C., Soengas, R.G., 2011. Iron(iii) complexation by
562 Vanchrobactin, a siderophore of the bacterial fish pathogen *Vibrio anguillarum*.
563 Metallomics 3, 521–528. https://doi.org/10.1039/c0mt00071j

564 India Science Wire, 2019. Scientists intervene to save dry toilets. Accessed April 18, 2020
565 http://vigyanprasar.gov.in/isw/Scientists-intervene-to-save-dry-toilets.html

566

567 Jurado, M.M., Suárez-Estrella, F., López, M.J., Vargas-García, M.C., López-González, J.A.,
568 Moreno, J., 2015. Enhanced turnover of organic matter fractions by microbial
569 stimulation during lignocellulosic waste composting. Bioresource Technology 186, 15–
570 24. https://doi.org/10.1016/j.biortech.2015.03.059

571 Karigar, C.S., Rao, S.S., 2011. Role of microbial enzymes in the bioremediation of
572 pollutants: A review. Enzyme Research 2011. https://doi.org/10.4061/2011/805187

573 Karthika, S., Midhun, S.J., Jisha, M.S., 2020. A potential antifungal and growth-promoting
574 bacterium *Bacillus* sp. KTMA4 from tomato rhizosphere. Microbial Pathogenesis 142,
575 104049. https://doi.org/10.1016/j.micpath.2020.104049

576 Kasana, R.C., Salwan, R., Dhar, H., Dutt, S., Gulati, A., 2008. A rapid and easy method for
577 the detection of microbial cellulases on agar plates using Gram's iodine. Current
578 Microbiology 57, 503–507. https://doi.org/10.1007/s00284-008-9276-8

579 Kostylev, M., Wilson, D., 2012. Synergistic interactions in cellulose hydrolysis. Biofuels 3,
580 61–70.

581 Krewulak, K.D., Vogel, H.J., 2016. Bacterial Siderophore-Binding Protein FepB.
582 Encyclopedia of Inorganic and Bioinorganic Chemistry 1–10.
583 https://doi.org/10.1002/9781119951438.eibc2441

584 Kumar, R., Singh, D., Swarnkar, M.K., Singh, A.K., Kumar, S., 2015. Genome assembly of
585 *Chryseobacterium polytrichastri* ERMR1:04, a psychrotolerant bacterium with cold
586 active proteases, isolated from east rathong glacier in India. Genome Announcements 3,
587 2014–2015. https://doi.org/10.1128/genomeA.01305-15

588 Kumar, R., Nongkhlaw, M., Acharya, C., Joshi, S.R., 2013. Uranium (U)-tolerant bacterial
589 diversity from U ore deposit of domiasiat in North-East India and its prospective
590 utilisation in bioremediation. Microbes and Environments 28, 33–41.
591 https://doi.org/10.1264/jsme2.ME12074

592 Kumar, S., Stecher, G., Tamura, K., 2016. MEGA7: Molecular Evolutionary Genetics
593 Analysis Version 7.0 for Bigger Datasets. Molecular biology and evolution 33, 1870–
594 1874. https://doi.org/10.1093/molbev/msw054

595 Kuniyal, J.C., Vishvakarma, S.C.R., Singh, G.S., 2004. Changing crop biodiversity and
596 resource use efficiency of traditional versus introduced crops in the cold desert of the
597 northwestern Indian Himalaya: A case of the Lahaul valley. Biodiversity and
598 Conservation 13, 1271–1304. https://doi.org/10.1023/B:BIOC.0000019404.48445.27

599 Larkin, M.A., Blackshields, G., Brown, N.P., Chenna, R., McGettigan, P.A., McWilliam, H.,
600 Valentin, F., Wallace, I.M., Wilm, A., Lopez, R., 2007. Clustal W and Clustal X version
601 2.0. bioinformatics 23, 2947–2948.

602 Li, M., Guo, R., Yu, F., Chen, X., Zhao, H., Li, H., Wu, J., 2018. Indole-3-acetic acid
603 biosynthesis pathways in the plant-beneficial bacterium *Arthrobacter pascens* zz21.
604 International Journal of Molecular Sciences 19. https://doi.org/10.3390/ijms19020443

605 Liao, L., Su, S., Zhao, B., Fan, C., Zhang, J., Li, H., Chen, B., 2019. Biosynthetic Potential of
606 a Novel Antarctic *Actinobacterium Marisediminicola antarctica* ZS314T Revealed by
607 Genomic Data Mining and Pigment Characterization. Marine Drugs 17, 1–15.
608 https://doi.org/10.3390/md17070388

609 Lynne, A.M., Haarmann, D., Louden, B.C., 2011. Use of Blue Agar CAS Assay for
610 Siderophore Detection. Journal of Microbiology & Biology Education 12, 51–53.
611 https://doi.org/10.1128/jmbe.v12i1.249

612 Mageswari, A., Subramanian, P., Chandrasekaran, S., Karthikeyan, S., Gothandam, K.M.,
613 2017. Systematic functional analysis and application of a cold-active serine protease
614 from a novel *Chryseobacterium* sp. Food Chemistry 217, 18–27.
615 https://doi.org/10.1016/j.foodchem.2016.08.064

616 Martínez-García, S., Rodríguez-Martínez, S., Cancino-Diaz, M.E., Cancino-Diaz, J.C., 2018.
617 Extracellular proteases of *Staphylococcus epidermidis*: roles as virulence factors and
618 their participation in biofilm. Apmis 126, 177–185. https://doi.org/10.1111/apm.12805

619 Monnet, C., Loux, V., Gibrat, J.F., Spinnler, E., Barbe, V., Vacherie, B., Gavory, F.,
620 Gourbeyre, E., Siguier, P., Chandler, M., Elleuch, R., Irlinger, F., Vallaeys, T., 2010. The
621 Arthrobacter arilaitensis Re117 genome sequence reveals its genetic adaptation to the
622 surface of cheese. PLoS ONE 5. https://doi.org/10.1371/journal.pone.0015489

623 Nordberg, H., Cantor, M., Dusheyko, S., Hua, S., Poliakov, A., Shabalov, I., Smirnova, T.,
624 Grigoriev, I. v., Dubchak, I., 2014. The genome portal of the Department of Energy
625 Joint Genome Institute: 2014 updates. Nucleic Acids Research 42, 26–31.
626 https://doi.org/10.1093/nar/gkt1069

627 Numan, M., Bashir, S., Khan, Y., Mumtaz, R., Shinwari, Z.K., Khan, A.L., Khan, A., AL-
628 Harrasi, A., 2018. Plant growth promoting bacteria as an alternative strategy for salt

629 tolerance in plants: A review. Microbiological Research 209, 21–32.
630 https://doi.org/10.1016/j.micres.2018.02.003

631 Oinam, S.S., 2008. Traditional night-soil composting continues to bring benefits. Leisa
632 Magazine 24, 25–27.

633 Oinam, S.S., Rawat, Y.S., Kuniyal, J.C., Vishvakarma, S.C.R., Pandey, D.C., 2008. Thermal
634 supplementing soil nutrients through biocomposting of night-soil in the northwestern
635 Indian Himalaya. Waste Management 28, 1008–1019.
636 https://doi.org/10.1016/j.wasman.2007.03.004

637 Oteino, N., Lally, R.D., Kiwanuka, S., Lloyd, A., Ryan, D., Germaine, K.J., Dowling, D.N.,
638 2015. Plant growth promotion induced by phosphate solubilising endophytic
639 *Pseudomonas* isolates. Frontiers in Microbiology 6, 1–9.
640 https://doi.org/10.3389/fmicb.2015.00745

641 Page, A.J., Cummins, C.A., Hunt, M., Wong, V.K., Reuter, S., Holden, M.T.G., Fookes, M.,
642 Falush, D., Keane, J.A., Parkhill, J., 2015. Roary: Rapid large-scale prokaryote pan
643 genome analysis. Bioinformatics 31, 3691–3693.
644 https://doi.org/10.1093/bioinformatics/btv421

645 Parks, D.H., Imelfort, M., Skennerton, C.T., Hugenholtz, P., Tyson, G.W., 2015. CheckM:
646 Assessing the quality of microbial genomes recovered from isolates, single cells, and
647 metagenomes. Genome Research 25, 1043–1055. https://doi.org/10.1101/gr.186072.114

648 Patterson, J.L., Stull-Lane, A., Girerd, P.H., Jefferson, K.K., 2010. Analysis of adherence,
649 biofilm formation and cytotoxicity suggests a greater virulence potential of *Gardnerella*
650 *vaginalis* relative to other bacterial-vaginosis-associated anaerobes. Microbiology 156,
651 392–399. https://doi.org/10.1099/mic.0.034280-0

652 Peralta, D.R., Adler, C., Corbalán, N.S., Paz García, E.C., Pomares, M.F., Vincent, P.A.,
653 2016. Enterobactin as part of the oxidative stress response repertoire. PLoS ONE 11, 1–
654 15. https://doi.org/10.1371/journal.pone.0157799

655 Penn, R., Ward, B.J., Strande, L., Maurer, M., 2018. Review of synthetic human faeces and
656 faecal sludge for sanitation and wastewater research. Water Research 132, 222–240.
657 https://doi.org/10.1016/j.watres.2017.12.063

Powell, S., Forslund, K., Szklarczyk, D., Trachana, K., Roth, A., Huerta-Cepas, J., Gabaldon, T., Rattei, T., Creevey, C., Kuhn, M., 2014. eggNOG v4. 0: nested orthology inference across 3686 organisms. Nucleic acids research 42, D231–D239.

Price, M.N., Dehal, P.S., Arkin, A.P., 2010. FastTree 2–approximately maximum-likelihood trees for large alignments. PloS one 5.

Ramakrishna, W., Yadav, R., Li, K., 2019. Plant growth promoting bacteria in agriculture: Two sides of a coin. Applied Soil Ecology 138, 10–18. https://doi.org/10.1016/j.apsoil.2019.02.019

Raymond, K.N., Dertz, E.A., Kim, S.S., 2003. Enterobactin: An archetype for microbial iron transport. Proceedings of the National Academy of Sciences of the United States of America 100, 3584–3588. https://doi.org/10.1073/pnas.0630018100

Rosier, A., Medeiros, F.H.V., Bais, H.P., 2018. Defining plant growth promoting rhizobacteria molecular and biochemical networks in beneficial plant-microbe interactions. Plant and Soil 428, 35–55. https://doi.org/10.1007/s11104-018-3679-5

Seemann, T., 2014. Prokka: Rapid prokaryotic genome annotation. Bioinformatics 30, 2068–2069. https://doi.org/10.1093/bioinformatics/btu153

Segata, N., Börnigen, D., Morgan, X.C., Huttenhower, C., 2013. PhyloPhlAn is a new method for improved phylogenetic and taxonomic placement of microbes. Nature Communications 4. https://doi.org/10.1038/ncomms3304

Shimizu, Y., Ogata, H., Goto, S., 2017. Type III polyketide synthases: functional classification and phylogenomics. ChemBioChem 18, 50–65.

Sullivan, M.J., Petty, N.K., Beatson, S.A., 2011. Easyfig: A genome comparison visualizer. Bioinformatics 27, 1009–1010. https://doi.org/10.1093/bioinformatics/btr039

Tatusov, R.L., 2000. The COG database: a tool for genome-scale analysis of protein functions and evolution. Nucleic Acids Research 28, 33–36. https://doi.org/10.1093/nar/28.1.33

Tutino, M.L., Parrilli, E., Giaquinto, L., Duilio, A., Sannia, G., Feller, G., Marino, G., 2002. Secretion of alpha-Amylase from. Society 184, 5814–5817. https://doi.org/10.1128/JB.184.20.5814

U.S. Composting Council. 2002. Test methods for the examination of composting and compost (TMECC). Accessed April 18, 2020. https://compostingcouncil.org/tmecc/

Vermelho, A.B., Couri, S., 2013. Methods to determine enzymatic activity. Bentham Science Publishers.

Wayne, P.A., 2011. Clinical and laboratory standards institute. Performance standards for antimicrobial susceptibility testing.

William, S., Feil, H., Copeland, A., 2004. Bacterial DNA Isolation CTAB Protocol Bacterial genomic DNA isolation using CTAB Materials & Reagents. Doe Joint Genome Institute 4.

Wilson, B.A., Winkler, M., Ho, B.T., 2019. Bacterial pathogenesis: a molecular approach. John Wiley & Sons.

Wortham, B.W., Oliveira, M.A., Patel, C.N., 2007. Polyamines in bacteria: Pleiotropic effects yet specific mechanisms. Advances in Experimental Medicine and Biology 603, 106–115. https://doi.org/10.1007/978-0-387-72124-8_9

Xiao, Z., Storms, R., Tsang, A., 2005. Microplate-based carboxymethylcellulose assay for endoglucanase activity. Analytical Biochemistry 342, 176–178. https://doi.org/10.1016/j.ab.2005.01.052

Yoon, S.H., Ha, S. min, Lim, J., Kwon, S., Chun, J., 2017. A large-scale evaluation of algorithms to calculate average nucleotide identity. Antonie van Leeuwenhoek, International Journal of General and Molecular Microbiology 110, 1281–1286. https://doi.org/10.1007/s10482-017-0844-4

Zhang, H., Yohe, T., Huang, L., Entwistle, S., Wu, P., Yang, Z., Busk, P.K., Xu, Y., Yin, Y., 2018. DbCAN2: A meta server for automated carbohydrate-active enzyme annotation. Nucleic Acids Research 46, W95–W101. https://doi.org/10.1093/nar/gky418

Zhang, Y., Ji, F., Wang, J., Pu, Z., Jiang, B., Bao, Y., 2018. Purification and characterization of a novel organic solvent-tolerant and cold-adapted lipase from *Psychrobacter* sp. ZY124. Extremophiles 22, 287–300. https://doi.org/10.1007/s00792-018-0997-8

715 Zhou, C., Ma, Z., Zhu, L., Xiao, X., Xie, Y., Zhu, J., Wang, J., 2016. Rhizobacterial strain
716 *Bacillus megaterium* BOFC15 induces cellular polyamine changes that improve plant
717 growth and drought resistance. International Journal of Molecular Sciences 17.
718 https://doi.org/10.3390/ijms17060976

719 Zhou, S., Zhang, X., Liao, X., Wu, Y., Mi, J., Wang, Y., 2019. Effect of different proportions
720 of three microbial agents on ammonia mitigation during the composting of layer
721 manure. Molecules 24, 1–18. https://doi.org/10.3390/molecules24132513

722

Figure captions

Fig. 1. Traditional winter dry toilet of Lahaul valley: A) Traditional winter dry toilet attached to the living room of the main house. The upper storey is used for defaecation, while lower storey is a collection chamber where composting takes place. **B)** Inside view of defaecation room. After defaecation people cover the faces with *fot* (dry cattle/sheep dung, kitchen ash, dry grass/leaves). C) Collection of night-soil compost (NSC) sample from the collection chamber. D) NSC pile dumped in open fields for further curing.

Fig. 2. Phylo-taxono-genomics of *Glutamicibacter arilaitensis* LJH19: **A)** 16S rRNA gene phylogeny obtained from the all available *Glutamicibacter* strains. **B)** ML based phylogenomic tree construction obtained from the whole proteome information of the strains of genus *Glutamicibacter*. Violet color circle at each node represents corresponding bootstrap values **C)** OrthoANI similarity matrix created with morpheous, red color represents the maximum values, and yellow color represents the minimum value whereas the green color is the intermediate values. Orange color represents the cutoff value for species demarcation (95% similarity).

Fig. 3. **Circular genome representation of LJH19: A)** BRIG implementation across the three closely related strains including type strain of species Re117, JB182 and LJH19, which resulted in the identification of the unique genomic region across the isolates LJH19. **B).** Unique genes were fetched from the strain LJH19 using pan genome analysis with the implementation of roary. COG classes and its count identified by eggnog, shows the prevalence of C: Energy production and conversion, E: Amino Acid metabolism and transport, G: Carbohydrate metabolism and transport, I: Lipid metabolism, K: Transcription, L: Replication and repair, M: Cell wall/membrane/envelop biogenesis, and P: Inorganic ion transport and metabolism.

Fig. 4. An overview of catabolic activities, transport and plant growth promotion in *G. arilaitensis* LJH19. Following are the selected key genes involved in the pathway : 1, amylase; 2, Oligo-1,6-glucosidase; 3, Beta-glucosidase; 4, Triacylglyceride lipase; 5, monoacylglycerol lipase ; 6, Anthranilate synthase component I (TrpE) ; 7, Anthranilate phosphoribosyl transferase (TrpD); 7,Phosphoribosyl anthranilate isomerase (TrpF); 9, Indole-3-glycerol phosphate synthase (TrpC); 11, Isochorismate synthase (menF); 12, Isochorismatase; 13, Amidase; 14, Argininosuccinate lyase (argH); 15, Arginine decarboxylase (speC); 16, Agmatinase (speB); 17, Polyamine aminopropyltransferase (speE);

18, Ornithine decarboxylase (speC)*. Red arrows indicate enzymes missing in the metabolic pathway. Multistep pathways are denoted with dotted lines.

* Gene was annotated as hypothetical protein in Prokka.

Fig. 5. Schematic depiction of unique genes involved in siderophore export, uptake and Ferric-enterobactin processing in LJH19 strain. The genes involved in petrobactin transport are apeX, Apo-petrobactin exporter; fatC/D, Petrobactin import system permease protein; fatE, Petrobactin import ATP-binding protein; yclQ, Petrobactin-binding protein. The genes involved in enterobactin transport are entS, Enterobactin exporter; fepD/G, Ferric enterobactin transport system permease protein; FepC, Ferric enterobactin transport ATP-binding protein; yfiY, putative siderophore-binding lipoprotein. Once translocated inside the bacterial cell, Fe-PB and Fe-EB are further processed by putative esterases to release iron and free PB and EB. Abbreviations are as follows: PUT, putrescine; SPD, spermidine; PB, petrobactin; EB, enterobactin; Fe-PB, ferric bound PB; Fe-EB ferric bound EB. (Hagan et al., 2017, 2016; Krewulak and Vogel, 2016).

Fig. 6. Biosynthetic gene cluster identified by the antiSMASH search namely type III polyketide synthase (PKS), terpene and siderophore. H represents the hypothetical gene cluster annotated by prokka. The direction of arrow represents the forward (5' → 3') and reverse orientation of the gene cluster. Among the type III PKS, terpene and siderophore, the predicted gene cluster shows significant hit with the other strains of the genus *Glutamicibacter*. A, B and C represents type III PKS, terpene and siderophore respectively.

775 **Table 1.** Physiological characterization, hydrolytic, plant growth promoting, and pathogenic
776 attributes of *G. arilaitensis* LJH19

777

Characteristic	***G. arilaitensis* LJH19**
Source	Night-soil compost
Growth condition	
Temperature range	15-37°C
pH range	7-8
NaCl	1%
Hydrolysis on agar plates	
Corn starch	+ ve (15)
Carboxymethylcellulose (CMC)	+ ve (5.66)
Birchwood xylan	+ ve (2.8)
Tributyrin	+ ve (1.8)
Enzyme assays	
Amylase	186.76 ± 19.28 U/mg
Cellulase	21.85 ± 0.7 U/mg
Xylanase	11.31± 0.51 U/mg
PGP trait	
IAA production	166.11 ± 5.7 µg/ml
Siderophore production	85.72 ± 1.06 psu
Phosphate solubilisation	44.76 ± 1.5 µg/ml
Ammonia production	0.20 ± 0.01 µmoles/ml
Pathogenic potential	
Haemolysis on blood agar	- ve
Protease production	0.17 ± 0.002 U/mg
Biofilm production	- ve at 37 °C, weak producer at 15 °C
Antibiotic susceptibility test	AZM^-, AMP^-, CIP^-, CHL^-, E^-, G^-, K^-, P^-, RIF^-, S^-, TE^-, VA^-

[a] Values in parentheses indicate enzymatic index (EI)
[+] Resistant
[-] Sensitive
Percent siderophore unit (psu)
15 mcg, Azithromycin (AZM); 10 mcg, Ampicillin (AMP); 5 mcg, Ciprofloxacin (CIP); 30 mcg, Chloramphenicol (CHL); 15 mcg Erythromycin (E); 10 mcg, Gentamycin (G); 30 mcg, Kanamycin (K); 10 Units, Penicillin-G (P); 5 mcg, Rifampicin (RIF); 10 mcg, Streptomycin (S); 30 mcg, Tetracycline (TE); 30 mcg, Vancomycin (VA)

778

779

780

781 **Table 2: Genome features of all the strain of *Glutamicibacter* sp. and strain LJH19 with its geographical attributes.**

Genome Name	Genome Status	Coverage (x)	# Contigs	Genome Length (bps)	% GC Content	# RefSeq CDS	Isolation source	%Completeness/ %Contamination	Accession No.
Glutamicibacter arilaitensis LJH19	WGS	153.0x	4	3602821	59.60	3245	Night soil compost	99.65/1.38	NZ_SPDS00000000
Glutamicibacter arilaitensis Re117	Complete	NA	2	3909664	59.28	3423	Cheese	99.74/0.46	NC_014550
Glutamicibacter soli M275	WGS	500.0x	319	3965931	64.09	3800	-	99.28/2.14	NZ_WYDN00000000
Glutamicibacter soli NHPC-3	WGS	100.0x	25	3840670	64.34	3495	Tea plant rhizospheric soil	99.28/0.69	NZ_POAF00000000
Glutamicibacter uratoxydans NBRC 15515	WGS	152.0x	49	3786014	61.09	3533	-	99.74/0.58	NZ_BJNY00000000
Glutamicibacter nicotianae NBRC 14234	WGS	162.0x	43	3554887	61.92	3311	-	99.74/1.19	NZ_BJNE00000000
Glutamicibacter nicotianae OTC-16	Complete	380.0x	3	3797724	61.72	-	Active sludge around pharmaceutical factory	99.28/1.53	NZ_CP033081
Glutamicibacter sp. JC586	WGS	100.0x	28	3524842	55.57	-	Soil	99.51/1.49	NZ_VHIN00000000
Glutamicibacter mysorens DSM 12798	WGS	34.0x	1	3459735	61.95	3177	-	99.74/0.96	NZ_PGEY00000000
Glutamicibacter arilaitensis JB182	WGS	50.0x	12	3947886	59.16	3708	Cheese rind	99.74/0.54	NZ_PNQX00000000

Glutamicibacter sp. HZAU	WGS	100.0x	40	3508313	61.70	3212	Bto:0003809	99.68/0.38	NZ_SCKZ00000000
Glutamicibacter sp. V16R2B1	WGS	12.0x	86	3479500	65.68	3197	Date palm rhizosphere	99.05/1.15	NZ_VATX00000000
Glutamicibacter sp. BW80	WGS	50.0x	78	4049569	60.38	3720	Cheese rind	99.74/0.61	NZ_NRGV00000000
Glutamicibacter sp. BW78	WGS	50.0x	43	3419483	64.04	3133	Cheese rind	99.77/0.61	NZ_NRGU00000000
Glutamicibacter sp. BW77	WGS	50.0x	90	3902028	56.57	3605	Cheese rind	99.51/0.5	NZ_NRGT00000000
Glutamicibacter halophytocola DR408	Complete	231.0x	1	3770186	60.19	3384	Rhizosphere of Soybean	99.51/1.15	NZ_CP042260
Glutamicibacter sp. 0426	WGS	241.0x	23	3549469	62		Soil	99.74/0.8	NZ_MPBI00000000
Glutamicibacter creatinolyticus LGCM 259	Complete	286.0x	1	3309128	65.55	2882	Abcess of a mare	99.51/0.69	NZ_CP034412
Glutamicibacter mysorens NBRC 103060	WGS	130.0x	15	3427456	62.02	-	-	99.74/0.96	NZ_BCQO00000000
Glutamicibacter sp. ZJUTW	Complete	100.0x	2	3673306	61.79	3379	Activated sludge	99.74/0.8	NZ_CP043624

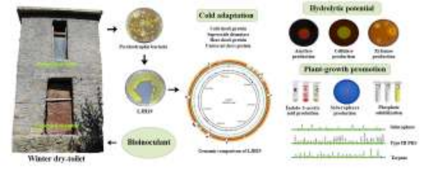
Cold adaptation
Hydrolytic potential
Plant-growth promotion
Bioinoculant
Winter dry-toilet

A.


Defaecation room
Main house
Collection chamber

B.


Fot

C.


NSC pile

D.

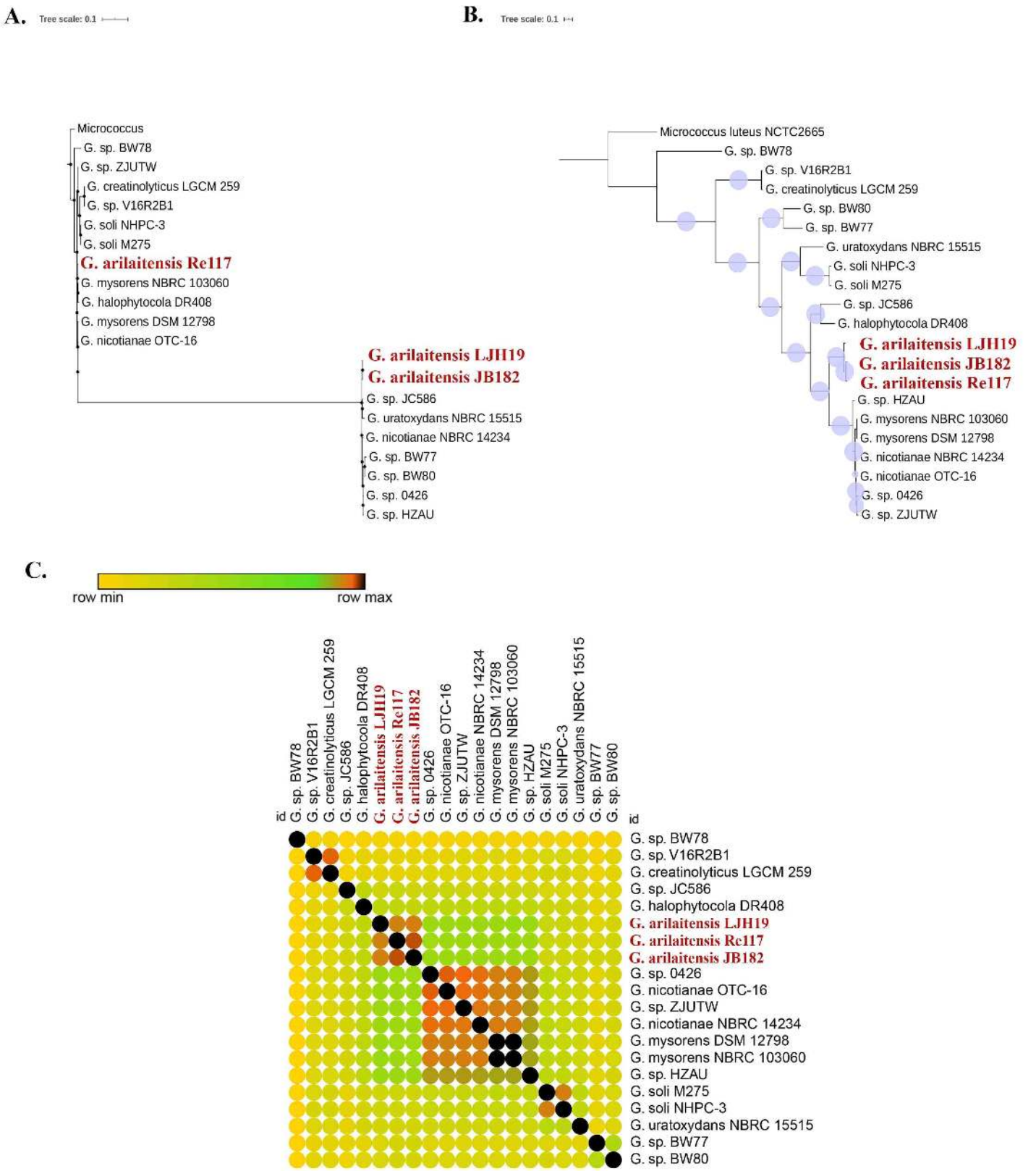
A.
Tree scale: 0.1
Micrococcus
G. sp. BW78
G. sp. ZJUTW
G. creatinolyticus LGCM 259
G. sp. V16R2B1
G. soli NHPC-3
G. soli M275
G. arilaitensis Re117
G. mysorens NBRC 103060
G. halophytocola DR408
G. mysorens DSM 12798
G. nicotianae OTC-16
G. arilaitensis LJH19
G. arilaitensis JB182
G. sp. JC586
G. uratoxydans NBRC 15515
G. nicotianae NBRC 14234
G. sp. BW77
G. sp. BW80
G. sp. 0426
G. sp. HZAU
B.
Tree scale: 0.1
Micrococcus luteus NCTC2665
G. sp. BW78
G. sp. V16R2B1
G. creatinolyticus LGCM 259
G. sp. BW80
G. sp. BW77
G. uratoxydans NBRC 15515
G. soli NHPC-3
G. soli M275
G. sp. JC586
G. halophytocola DR408
G. arilaitensis LJH19
G. arilaitensis JB182
G. arilaitensis Re117
G. sp. HZAU
G. mysorens NBRC 103060
G. mysorens DSM 12798
G. nicotianae NBRC 14234
G. nicotianae OTC-16
G. sp. 0426
G. sp. ZJUTW
C.
row min
row max
id
G. sp. BW78
G. sp. V16R2B1
G. creatinolyticus LGCM 259
G. sp. JC586
G. halophytocola DR408
G. arilaitensis LJH19
G. arilaitensis Re117
G. arilaitensis JB182
G. sp. 0426
G. nicotianae OTC-16
G. sp. ZJUTW
G. nicotianae NBRC 14234
G. mysorens DSM 12798
G. mysorens NBRC 103060
G. sp. HZAU
G. soli M275
G. soli NHPC-3
G. uratoxydans NBRC 15515
G. sp. BW77
G. sp. BW80
id

A.

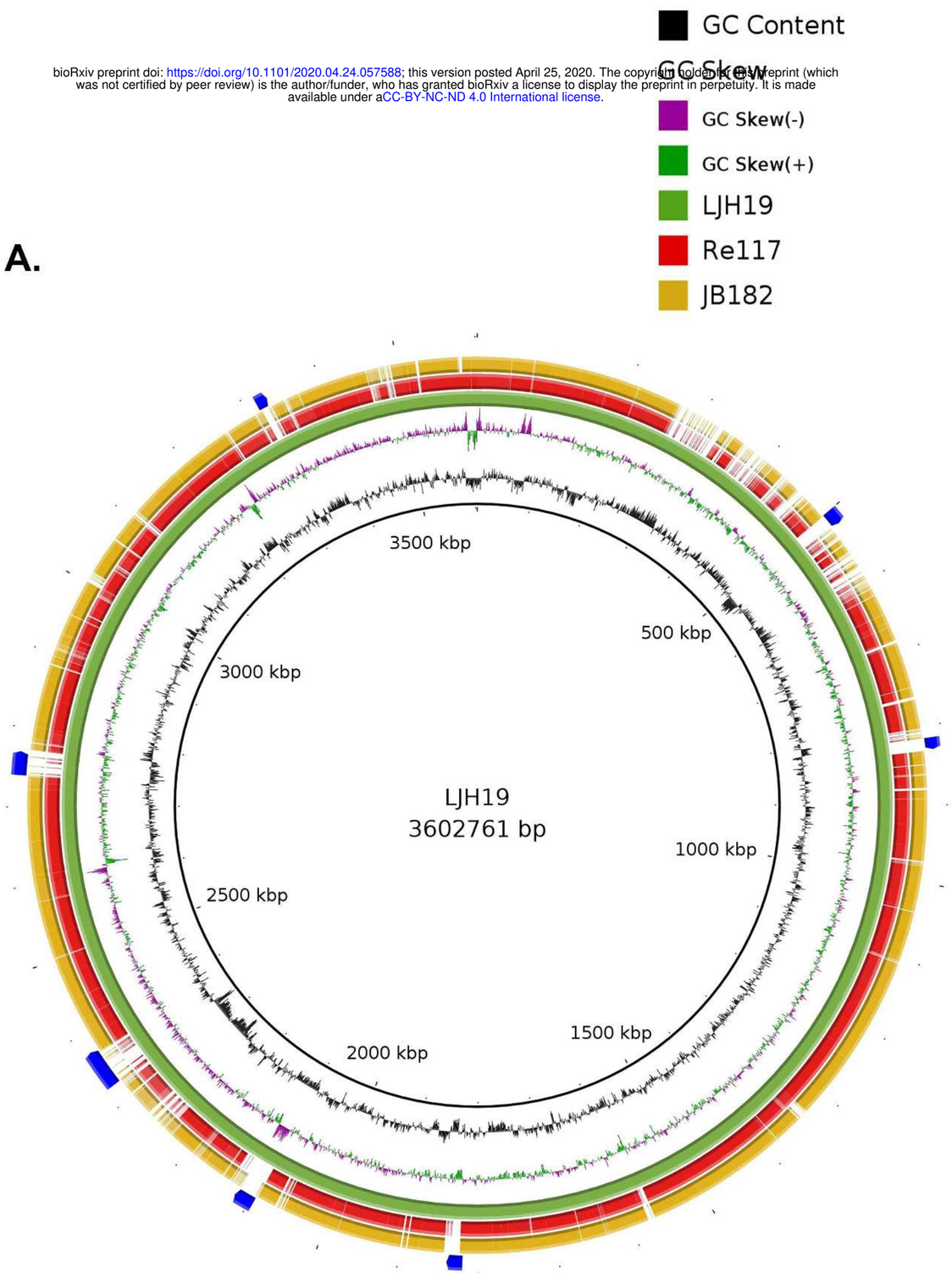

B.

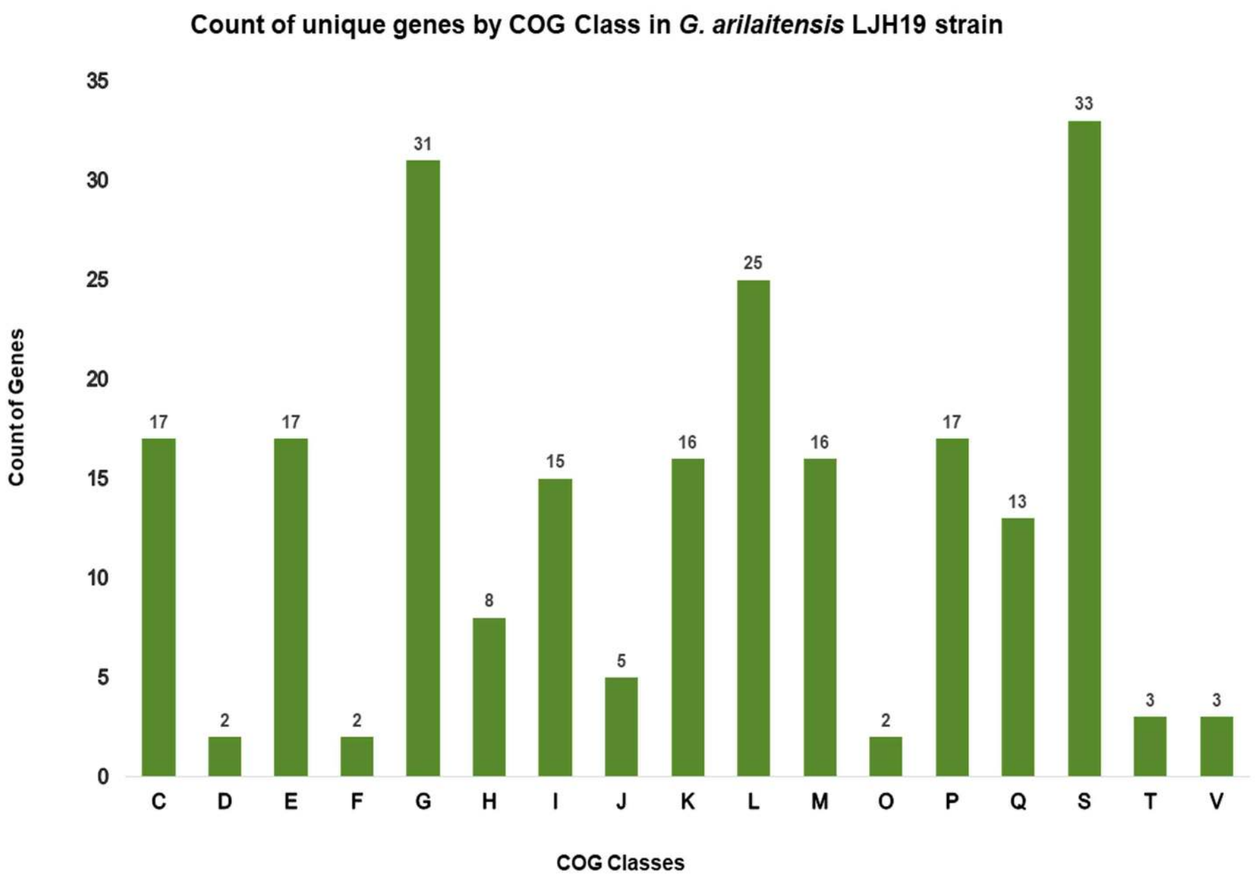

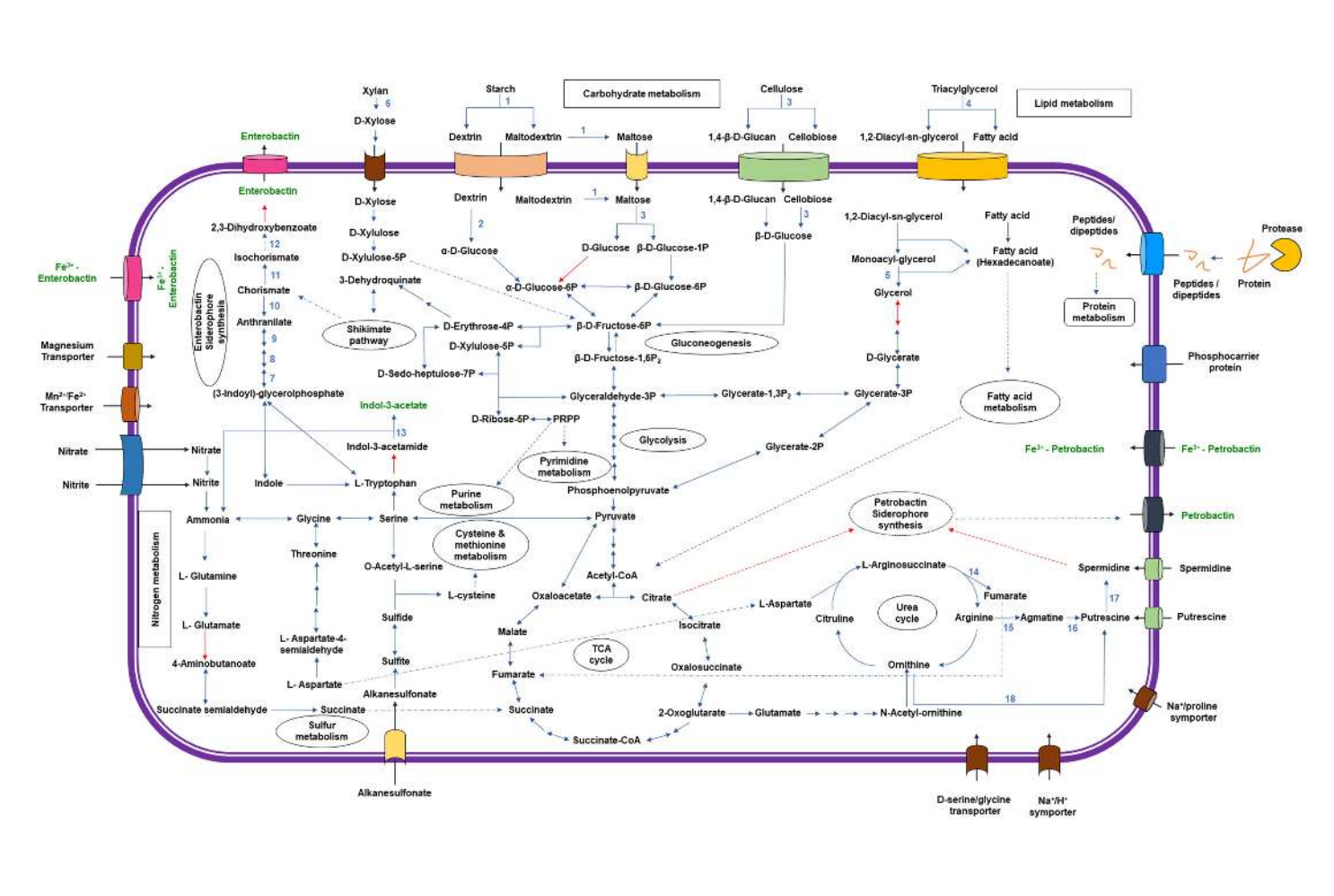
Carbohydrate metabolism
Lipid metabolism
Xylan
D-Xylose
Starch
Dextrin
Maltodextrin
Maltose
Cellulose
1,4-β-D-Glucan
Cellobiose
Triacylglycerol
1,2-Diacyl-sn-glycerol
Fatty acid
Enterobactin
Enterobactin
D-Xylose
Dextrin
Maltodextrin
Maltose
1,4-β-D-Glucan
Cellobiose
1,2-Diacyl-sn-glycerol
Fatty acid
Peptides/ dipeptides
Protease
Peptides / dipeptides
Protein
Protein metabolism
2,3-Dihydroxybenzoate
D-Xylulose
α-D-Glucose
D-Glucose
β-D-Glucose-1P
β-D-Glucose
Monoacyl-glycerol
Fatty acid (Hexadecanoate)
Fe³⁺ - Enterobactin
Fe³⁺ - Enterobactin
Isochorismate
D-Xylulose-5P
α-D-Glucose-6P
β-D-Glucose-6P
Glycerol
Enterobactin Siderophore synthesis
Chorismate
3-Dehydroquinate
Shikimate pathway
β-D-Fructose-6P
Gluconeogenesis
Phosphocarrier protein
Magnesium Transporter
Anthranilate
D-Erythrose-4P
D-Xylulose-5P
β-D-Fructose-1,6P2
D-Glycerate
Mn²⁺/Fe²⁺ Transporter
(3-Indoyl)-glycerolphosphate
D-Sedo-heptulose-7P
Glyceraldehyde-3P
Glycerate-1,3P2
Glycerate-3P
Fatty acid metabolism
Indol-3-acetate
D-Ribose-5P
PRPP
Glycolysis
Nitrate
Nitrate
Indol-3-acetamide
Pyrimidine metabolism
Glycerate-2P
Fe³⁺ - Petrobactin
Fe³⁺ - Petrobactin
Nitrite
Nitrite
Indole
L-Tryptophan
Purine metabolism
Phosphoenolpyruvate
Petrobactin Siderophore synthesis
Petrobactin
Ammonia
Glycine
Serine
Pyruvate
Nitrogen metabolism
Cysteine & methionine metabolism
Threonine
O-Acetyl-L-serine
Acetyl-CoA
L-Arginosuccinate
Spermidine
Spermidine
L- Glutamine
L-cysteine
Oxaloacetate
Citrate
L-Aspartate
Fumarate
Urea cycle
Arginine
Agmatine
Putrescine
Putrescine
L- Glutamate
Sulfide
Malate
Isocitrate
Citrulline
L- Aspartate-4-semialdehyde
TCA cycle
Oxalosuccinate
Ornithine
4-Aminobutanoate
Sulfite
Fumarate
L- Aspartate
Alkanesulfonate
Succinate semialdehyde
Succinate
Succinate
2-Oxoglutarate
Glutamate
N-Acetyl-ornithine
Na⁺/proline symporter
Sulfur metabolism
Succinate-CoA
Alkanesulfonate
D-serine/glycine transporter
Na⁺/H⁺ symporter

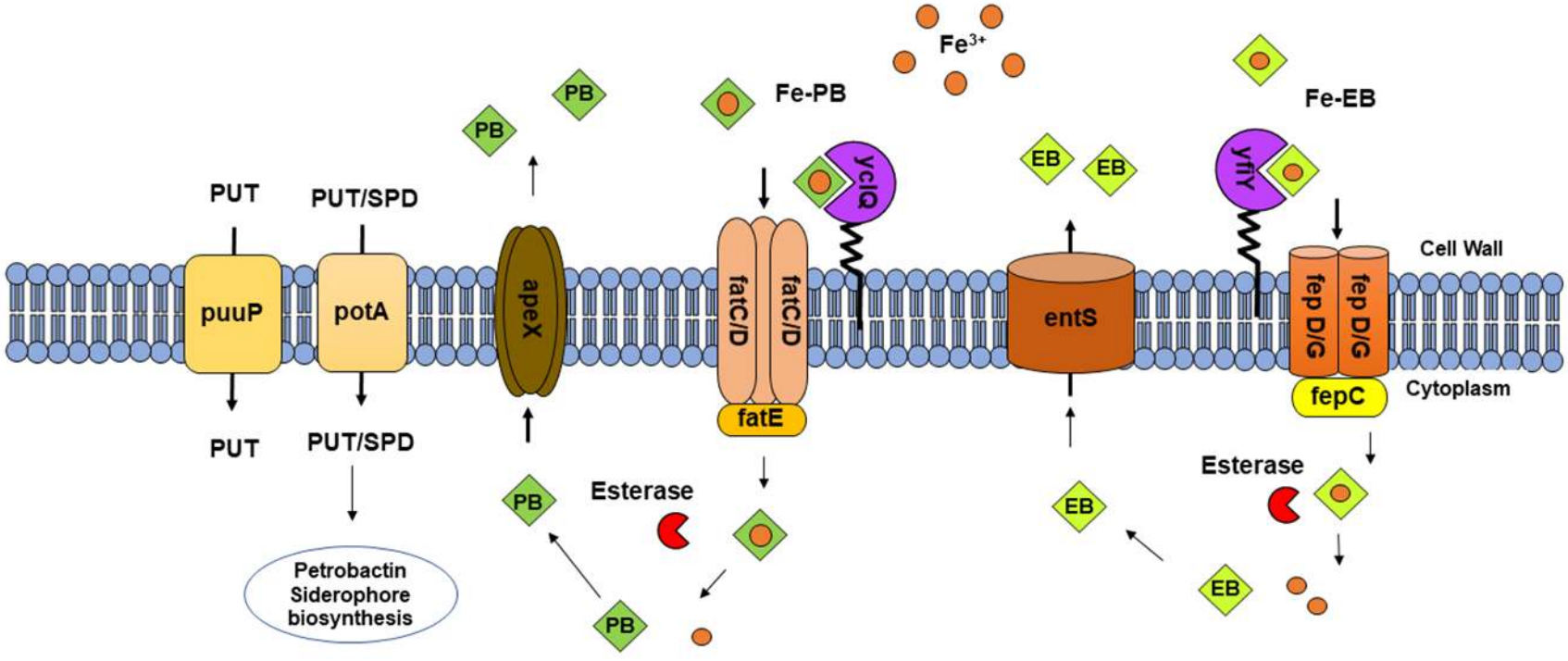
PUT
PUT/SPD
puuP
potA
PUT
PUT/SPD
Petrobactin
Siderophore
biosynthesis
PB
PB
apeX
PB
Esterase
PB
Fe-PB
fatC/D
fatC/D
fatE
yclQ
Fe3+
EB
EB
entS
EB
Esterase
EB
Fe-EB
yfiY
fep D/G
fep D/G
fepC
Cell Wall
Cytoplasm

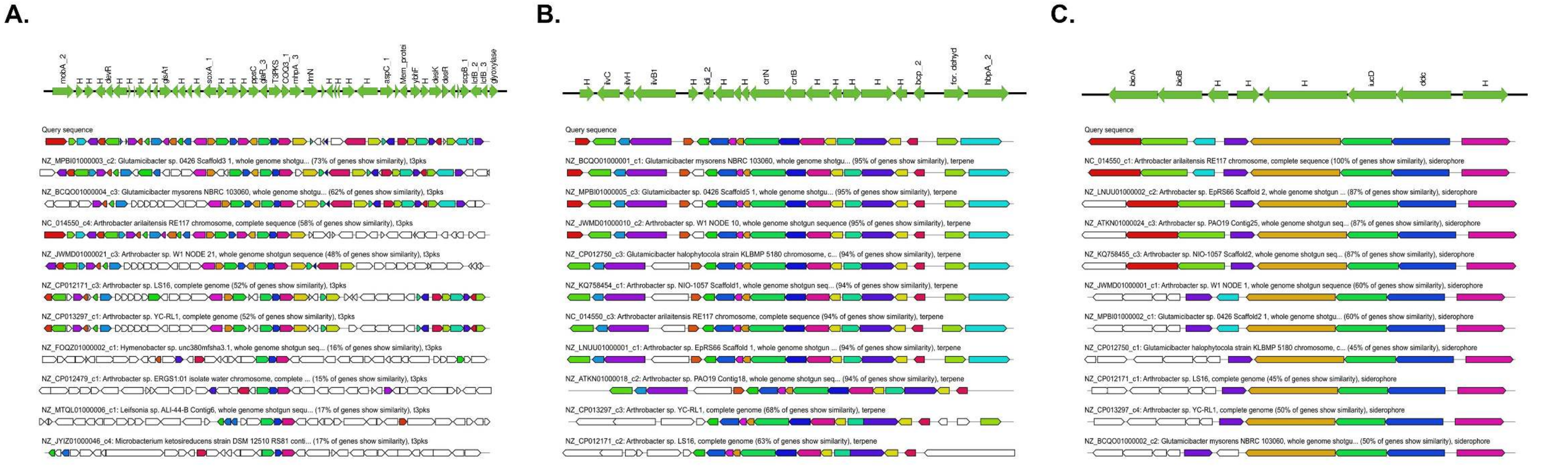
A.
motA_2
H
H
devR
H
H
H
gltA1
H
H
soxA_1
H
H
H
ppsC
gltR_3
T3PKS
COQ3_1
rnhpA_3
trmN
H
H
H
H
aspC_1
Mem_protei
ybhF
H
desK
desR
scpB_1
ictB_2
ictB_3
glyoxylase
Query sequence
NZ_MPBI01000003_c2: Glutamicibacter sp. 0426 Scaffold3 1, whole genome shotgu... (73% of genes show similarity), t3pks
NZ_BCQO01000004_c3: Glutamicibacter mysorens NBRC 103060, whole genome shotgu... (62% of genes show similarity), t3pks
NC_014550_c4: Arthrobacter arilaitensis RE117 chromosome, complete sequence (58% of genes show similarity), t3pks
NZ_JWMD01000021_c3: Arthrobacter sp. W1 NODE 21, whole genome shotgun sequence (48% of genes show similarity), t3pks
NZ_CP012171_c3: Arthrobacter sp. LS16, complete genome (52% of genes show similarity), t3pks
NZ_CP013297_c1: Arthrobacter sp. YC-RL1, complete genome (52% of genes show similarity), t3pks
NZ_FOQZ01000002_c1: Hymenobacter sp. unc380mfsha3.1, whole genome shotgun seq... (16% of genes show similarity), t3pks
NZ_CP012479_c1: Arthrobacter sp. ERGS1:01 isolate water chromosome, complete ... (15% of genes show similarity), t3pks
NZ_MTQL01000006_c1: Leifsonia sp. ALI-44-B Contig6, whole genome shotgun sequ... (17% of genes show similarity), t3pks
NZ_JYIZ01000046_c4: Microbacterium ketosireducens strain DSM 12510 RS81 conti... (17% of genes show similarity), t3pks
B.
H
ilvC
ilvH
ilvB1
H
idi_2
H
H
crtN
crtB
H
H
H
H
H
bcp_2
for. dehyd
hbpA_2
Query sequence
NZ_BCQO01000001_c1: Glutamicibacter mysorens NBRC 103060, whole genome shotgu... (95% of genes show similarity), terpene
NZ_MPBI01000005_c3: Glutamicibacter sp. 0426 Scaffold5 1, whole genome shotgu... (95% of genes show similarity), terpene
NZ_JWMD01000010_c2: Arthrobacter sp. W1 NODE 10, whole genome shotgun sequence (95% of genes show similarity), terpene
NZ_CP012750_c3: Glutamicibacter halophytocola strain KLBMP 5180 chromosome, c... (94% of genes show similarity), terpene
NZ_KQ758454_c1: Arthrobacter sp. NIO-1057 Scaffold1, whole genome shotgun seq... (94% of genes show similarity), terpene
NC_014550_c3: Arthrobacter arilaitensis RE117 chromosome, complete sequence (94% of genes show similarity), terpene
NZ_LNUU01000001_c1: Arthrobacter sp. EpRS66 Scaffold 1, whole genome shotgun ... (94% of genes show similarity), terpene
NZ_ATKN01000018_c2: Arthrobacter sp. PAO19 Contig18, whole genome shotgun seq... (94% of genes show similarity), terpene
NZ_CP013297_c3: Arthrobacter sp. YC-RL1, complete genome (68% of genes show similarity), terpene
NZ_CP012171_c2: Arthrobacter sp. LS16, complete genome (63% of genes show similarity), terpene
C.
bioA
bioB
H
H
H
iucD
ddc
H
Query sequence
NC_014550_c1: Arthrobacter arilaitensis RE117 chromosome, complete sequence (100% of genes show similarity), siderophore
NZ_LNUU01000002_c2: Arthrobacter sp. EpRS66 Scaffold 2, whole genome shotgun ... (87% of genes show similarity), siderophore
NZ_ATKN01000024_c3: Arthrobacter sp. PAO19 Contig25, whole genome shotgun seq... (87% of genes show similarity), siderophore
NZ_KQ758455_c3: Arthrobacter sp. NIO-1057 Scaffold2, whole genome shotgun seq... (87% of genes show similarity), siderophore
NZ_JWMD01000001_c1: Arthrobacter sp. W1 NODE 1, whole genome shotgun sequence (60% of genes show similarity), siderophore
NZ_MPBI01000002_c1: Glutamicibacter sp. 0426 Scaffold2 1, whole genome shotgu... (60% of genes show similarity), siderophore
NZ_CP012750_c1: Glutamicibacter halophytocola strain KLBMP 5180 chromosome, c... (45% of genes show similarity), siderophore
NZ_CP012171_c1: Arthrobacter sp. LS16, complete genome (45% of genes show similarity), siderophore
NZ_CP013297_c4: Arthrobacter sp. YC-RL1, complete genome (50% of genes show similarity), siderophore
NZ_BCQO01000002_c2: Glutamicibacter mysorens NBRC 103060, whole genome shotgu... (50% of genes show similarity), siderophore